Transportation Geotechnics 38 (2023) 100902

Contents lists available at ScienceDirect

Transportation Geotechnics

journal homepage: www.elsevier.com/locate/trgeo

Cross-Shear Test for geosynthetic-reinforced asphalt

G.H. Roodi [a,*], J.G. Zornberg [b], L. Yang [b], V.V. Kumar [b]

[a] HDR, 255 Adelaide St West, Toronto, Ontario M5H 1X9, Canada
[b] Department of Civil, Architectural, and Environmental Engineering, The University of Texas at Austin, 301 E. Dean Keeton St. Stop C1792, Austin, TX 78712, United States

ARTICLE INFO

Keywords:
Asphalt overlay
Geosynthetic reinforcement
Polymeric reinforcement
Glass reinforcement
Cross-shear test
Paving interlayers

ABSTRACT

Geosynthetics have been used within hot mix asphalt to provide a broad range of benefits, including those of controlling the development of reflective cracks into structural overlays, minimizing moisture infiltration, and increasing structural capacity. The performance of geosynthetic-reinforced asphalt has been evaluated under several loading modes through a variety of experimental procedures (e.g., three- and four-point bending, interface shear, wheel tracking test). However, limited research has been conducted to evaluate the performance of geosynthetic-reinforced asphalt under the shear loading mode that governs the reflection of cracks into structural overlays, which is shearing across the geosynthetic plane (cross-shear loading). In this study, an experimental procedure was developed to test the unreinforced and geosynthetic-reinforced asphalt subjected to cross-shear loading. Specifically, monotonic and cyclic cross-shear tests were conducted on control (unreinforced) asphalt specimens as well as asphalt specimens that were reinforced with four different geosynthetic reinforcements, including two polymeric and two glass products. The results show that all the geosynthetic reinforcements adopted in this study led to a significant improvement in the performance of asphalt specimens, though differences could be identified on the type of benefits provided by different geosynthetic products. Specifically, the geosynthetic with the highest tensile stiffness was found to provide the most significant benefits before crack development, but negligible post-cracking benefit due to its low elongation at break. On the other hand, comparatively less stiff geosynthetics showed significantly high post-cracking benefits. Under cyclic loading, while all reinforced asphalt specimens exhibited superior performance against the control specimens, the polymer-reinforced specimens showed comparatively better performance than the glass-reinforced specimens due to the better fatigue resistance of polymers as compared to glass.

Introduction

The use of paving interlayers, now a common approach to enhance the flexible pavements performance, aims at providing reinforcement, stiffening, stress relief, separation, and moisture barrier (e.g., [2,19,37,38]). Adequate incorporations of paving interlayers within the asphalt layer have been reported to provide several benefits that includes reduction in rutting (e.g., [4,7,15,24]), alleviation of reflective cracks (e.g., [13,14,28,34]), and enhancement of fatigue life (e.g., [9,16,26,30]). In circumstances that debonding occurs between asphalt and paving interlayers, the stiffness and structural capacity of the pavement may decrease (e.g., [29]). However, in conditions that do not lead to debonding, paving interlayers have been reported to provide additional benefits in terms of increased structural capacity that may result in the reduction of asphalt thickness and extended service life (e.g., [7,10,15,16,36]). However, the properties and conditions that determine the suitability of various types of geosynthetics used as paving interlayers still remain unclear, and specifications for these products often involve only descriptive characteristics rather than performance-based properties.

Although several experimental studies have been conducted to understand and characterize the performance of geosynthetic-reinforced asphalt under various modes of loading, comparatively limited research has been conducted to evaluate such performance under shear loads that are applied perpendicular to the reinforcement plane. Such shear loads correspond to a critical loading mode that is relevant to control reflective cracking. In this study, a new shear testing device and procedure was developed in which asphalt specimens are subjected to shear loads that are applied perpendicular to the reinforcement plane, referred herein as the cross-shear load. The significance of

* Corresponding author.
E-mail address: gholamhossein.roodi@hdrinc.com (G.H. Roodi).

https://doi.org/10.1016/j.trgeo.2022.100902
Received 11 December 2021; Received in revised form 6 June 2022; Accepted 6 November 2022
Available online 12 November 2022

understanding the benefits derived from geosynthetic reinforcements under this loading procedure is discussed in the next section. Practicality of the developed procedure and its capability to identify differences among various interface configurations were examined in monotonic and cyclic loading schemes to test control (unreinforced) asphalt specimens as well as asphalt specimens that were reinforced using four different geosynthetics, including polymeric and glass grids. Relevant parameters and protocols to evaluate experimental data in each loading scheme were developed. Using the data obtained in the monotonic and cyclic cross-shear tests, preliminary responses of different reinforcement types are discussed.

Background

One of the main objectives of incorporating interlayers below the asphalt overlay is to minimize reflective cracking.The two common approaches to achieve this objective include: 1) the development of tensile forces (reinforcement) in order to redistribute the stress concentration leading to the triggering of cracks; and 2) providing stress relief, which involves minimizing the shear transfer between preexisting asphalt layer and new asphalt overlay. However, the mechanisms that contribute to one approach are quite different from those contributing to the other, and, consequently, the properties to evaluate the suitability of interlayers for one approach can differ from those for another. While a stiff geosynthetic and a strong bond between geosynthetic and adjacent asphalt layers are essential to develop the tension required to induce the reinforcement, a comparatively less stiff geosynthetic that also reduces the bond between the asphalt layers is required to accomplish stress relief.

The multifaceted nature of loads applied on the pavement structure results complex stress and strain patterns in the various pavement layers. Traffic and environmental loads have been identified as the two main sources of pavement stresses that may lead to possible failures in the various structural layers. Fig. 1 shows a schematic of changes in the vertical normal stress (σ_v), horizontal normal stress (σ_h), and shear stresses (τ) induced by a moving wheel load at any point within the asphalt layer in a flexible pavement [6,17]. The time history of the normal and shear stresses acting on the horizontal and vertical planes under a moving wheel load are as shown in Fig. 1(b). As the wheel approaches, the normal stresses in the vertical and horizontal planes at Point A increases and reaches a maximum value when the wheel is atop Point A, and eventually reduces as the wheel departs from Point A. On the other hand, the shear stresses on the vertical plane increases to a maximum value when the wheel approaches Point A and subsequently reduces to zero when the wheel load is located exactly atop Point A.

However, the actual state of the stresses in pavement layers could be more complex than the stress pattern exhibited in Fig. 1. For example, the thermal strains induced by daily and seasonal temperature variations would affect the stress pattern in the asphalt layer (e.g., [19]). More importantly, initiation and propagation of cracks and other forms of distresses in the asphalt layer would significantly affect the stress field in the vicinity of such distresses.

The performance of a structural overlay may be significantly influenced by the presence or absence of cracks in the preexisting asphalt layer resulting in stress patterns that can be quite different than those presented in Fig. 1. In case of the overlays that are placed on an underlying cracked asphalt layer, traffic and thermal loads induce stress concentrations in the vicinity of cracks that may trigger propagation of cracks into the asphalt overlay. The three main stress patterns that result in the propagation of cracks have been classified in fracture mechanics as follows (Irwin [12]):

1) Mode I: Opening mode (or tensile cracks), in which tensile stresses are applied in the direction normal to the plane of the crack (Fig. 2a)
2) Mode II: Sliding mode (or transverse shear cracks), in which shear stresses are applied parallel to the plane of the crack (i.e., perpendicular to the crack propagation front (Fig. 2b)
3) Mode III: Tearing mode (or longitudinal shear cracks), in which shear stresses are applied in a direction that is parallel to that of the crack propagation front (Fig. 2c)

One of the experimental procedures that has been adopted to evaluate the performance of unreinforced and reinforced asphalt involves flexing an asphalt specimen repeatedly where the induced stresses are consistent with the pattern illustrated by the opening mode. Such tests include three- or four-point beam tests (Fig. 3a) and plate load tests (Fig. 3b) (e.g., [4,13,11,14,15,26,29,30]). In these experiments, load is applied on unreinforced and reinforced asphalt beams or slabs to induce tensile stresses that results in a maximum tensile strain at the bottom of the asphalt layer that is responsible for crack initiation and propagation into the asphalt overlay. Intact and pre-notched specimens have been used to assess the propagation of pre-existing cracks and evaluate the overall performance of overlays (e.g., [13,25–26,29,30,31]). Additional experiments have used moving wheels to simulate traffic passes, which induce stress fields that are representative of those occurring under actual traffic loads (Fig. 3c) (e.g., [7–8,24]). While the results obtained using such test devices attempt to reproduce the different types of solicitations that may affect the roadway performance, differentiation of the impact of each one of such stress types has been difficult to achieve. Studies have also been conducted to characterize the interface bond strength between paving interlayers and the adjacent asphalt layers that involved direct or torsional shear configurations as well as pullout

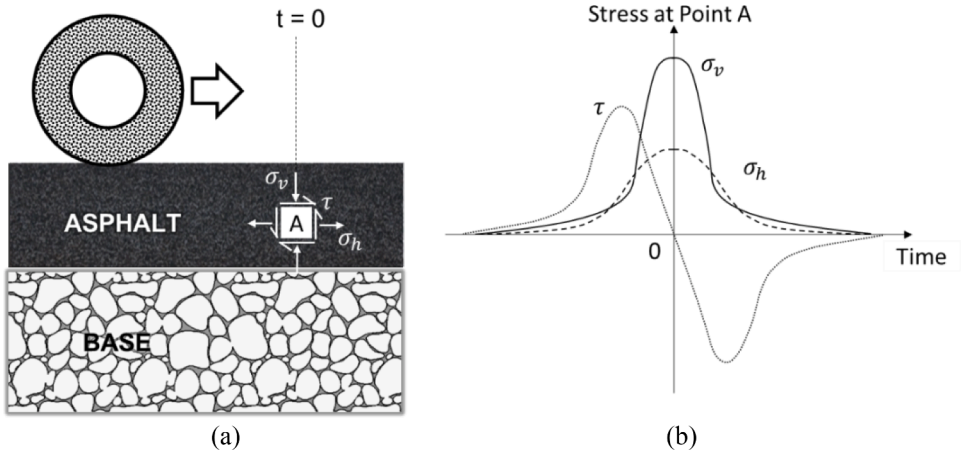

Fig. 1. Stress changes within an asphalt layer under a moving wheel load: (a) Schematic view; (b) Time history of normal and shear stresses (adapted from [17] and [6]).

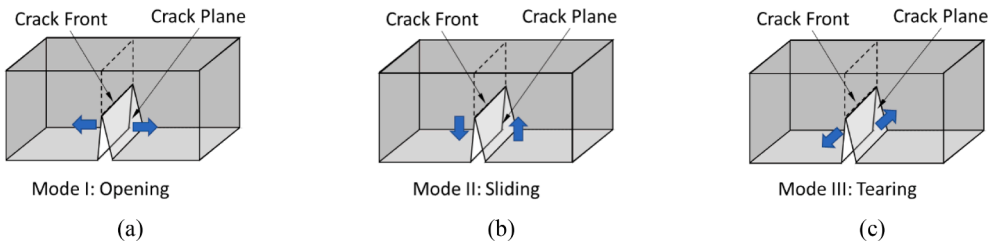

Fig. 2. Three independent stress patterns resulting in propagation of cracks: a) Mode I, opening mode; b) Mode II, sliding mode; and c) Mode III, tearing mode.

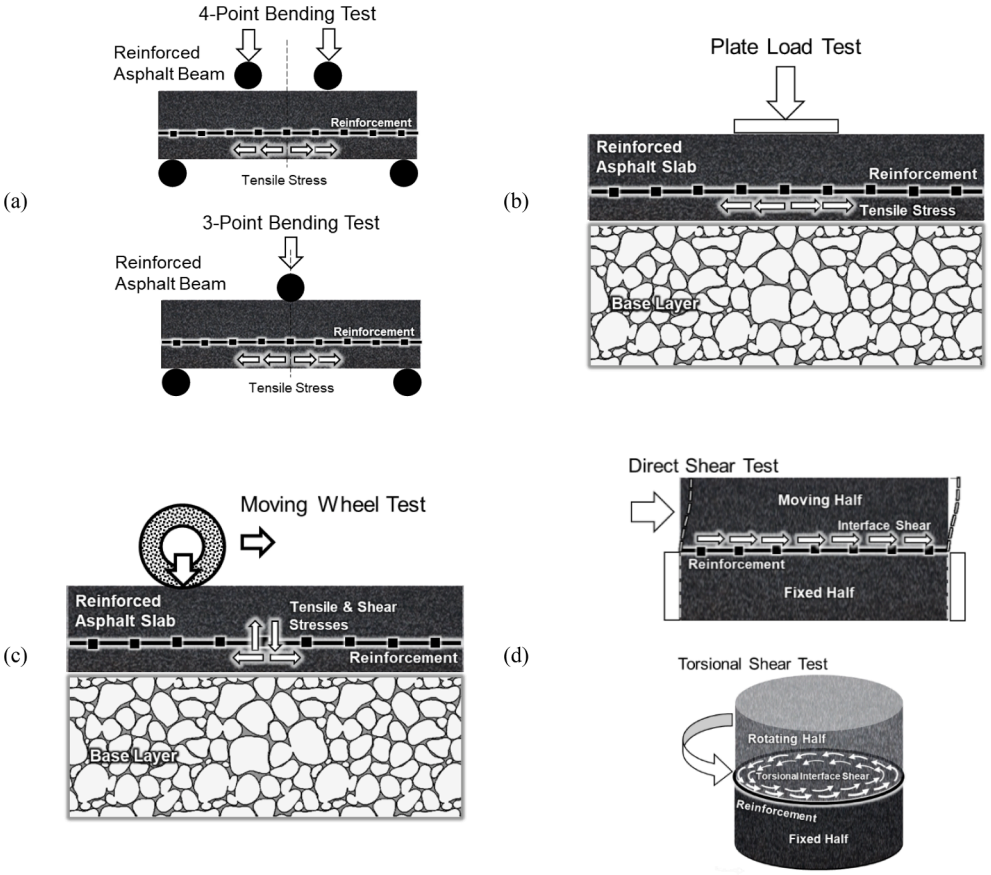

Fig. 3. Experimental procedures that have been used to evaluate reinforced asphalt: a) three- and four-point bending test; b) plate load tests; c) moving wheel tests; and d) interface tests (direct and torsional shear).

loading approaches. In these tests, shear is induced parallel to the reinforcement-asphalt interface to evaluate the bond strength at the interface (Fig. 3d) (e.g., [5,18,23,25,28,29,32]).

However, limited research has adopted a loading mechanism governed by shear stresses that are applied perpendicular to the geosynthetic reinforcement plane, referred to as the cross-shear stress. Such shear stresses constitute an important mechanism for the reflection of cracks from an old underlying into the new overlaying pavement, corresponding to the sliding mode of crack propagation (Fig. 2b). The test developed in this study, referred to as the cross-shear test, uses an experimental procedure to isolate and characterize the benefits derived from paving interlayers under cross-shear stresses. The cross-shear stresses may be induced by wheel loads (Fig. 1) or other sources that cause differential vertical movements. The asphalt overlays constructed over an asphalt surface with preexisting cracks are subjected to differential vertical movements between the two sides of the cracks. This condition may also be expected when an asphalt overlay is placed on a jointed concrete pavement that has expansion/contraction joints. Temperature loads, inconsistencies in roadway construction, and foundation problems can also induce differential vertical movements in asphalt. Specifically, roadways constructed along areas with significant changes in the subgrade properties or those founded over problematic subgrades (e.g., expansive clay subgrades, subgrades that are subjected to freeze–thaw cycles) are particularly prone to differential vertical movements resulting the development of cross-shear stresses.

Development of Cross-shear Test

The cross-shear device developed in this study allows testing of brick-shaped asphalt specimens, with or without geosynthetic reinforcement, measuring 150 mm × 75 mm × 38 mm. As illustrated in Fig. 4, one half of the specimen is fixed, while the other half can displace vertically. The bottom of the fixed half of the specimen is attached with epoxy to a steel plate measuring 150 mm × 100 mm (and 12.5 mm in thickness), while a steel plate of the same size is placed on top of this half without epoxy. The top of the moving half of the specimen is attached with epoxy to a steel plate measuring 150 mm × 100 mm (and 22 mm in thickness), while the bottom of this half is free. A gap of 5 mm is used

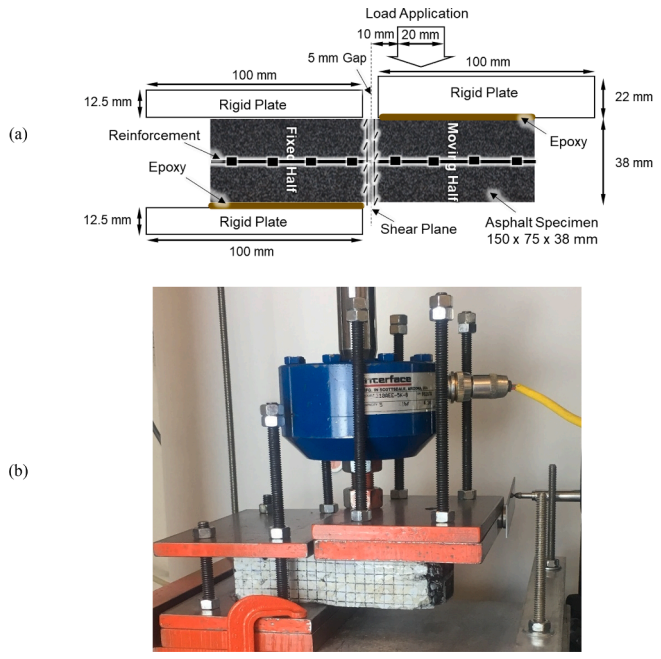

Fig. 4. Asphalt cross-shear test: a) schematic layout; b) experimental setup.

between the plates attached to the two halves of the specimen. This setup is similar to that used in the asphalt overlay tester [35] except that the steel plates are attached to the opposite sides of the asphalt specimen. The bottom plate of the fixed half of the asphalt specimen is screwed to the bottom platform, while the moving half is loaded by attaching the top plate to a loading arm. Vertical loading on the moving half of the specimen induces shear loading in the cross section of the asphalt specimen located between the fixed and moving specimen halves.

Test Specimens

The brick-shaped asphalt specimens adopted in this study are cut from laboratory-prepared cylindrical asphalt samples. The cylindrical samples are initially prepared in two halves representing two asphalt layers. In the case of a project involving reinforcement of a new asphalt layer, the bottom half represents the bottom asphalt lift while the top half represents the overlain asphalt lift. In the case of a project involving reinforcement of an asphalt overlay, the bottom half represents the old asphalt while the top half represents an asphalt overlay.

The asphalt mixture of the bottom layer is first prepared by mixing the preheated aggregates and binder. The asphalt mixture is then poured into a steel mold with 150 mm diameter and compacted using a servo-controlled gyratory compactor to the target density. The compacted bottom layer is allowed to cool for 24 hours. The tack coat emulsion is then applied (Fig. 5a) and the geosynthetic reinforcement is cut and placed (only in reinforced specimens) after the emulsion breaks (Fig. 5b). The geosynthetic reinforcement is cut to fit the circular cross-section of the asphalt specimen. A nominal weight of 2.25 kg is placed atop the reinforcement and left for an hour. This weight and the waiting time were adopted after experimental trials aiming at securing geosynthetic on the bottom asphalt layer without bleeding of underlying tack coat. The top asphalt layer is then placed and compacted (Fig. 5c). The diameter and height of the full cylindrical specimens are 150 and 114 mm, respectively.

The cylindrical sample is then trimmed to the brick-shaped test specimen shown in Fig. 6. Following trimming, the dimensions of the specimen should be 150 mm in maximum length (original diameter), 75 mm in width, and 38 mm in thickness.

Setup Design

Several experimental layouts were evaluated to optimize the experimental setup and testing procedure. This section provides not only the finally adopted testing methods but also some of the evaluations that led to the final selection.

Gripping of the Asphalt Specimen

Considering the viscoelastic response of asphalt mix materials, it was deemed necessary to avoid compressing the asphalt specimen when gripping it for subsequent testing. This was a concern with an initial experimental layout considered in this study that involved metal plates on top and bottom of both halves of the asphalt specimen, tightened using screws to fix the specimen between the plates. Instead, the finally selected experimental layout involved using epoxy to attach each asphalt specimen to the plates on one side only. As depicted in Fig. 4, the top of the moving half and the bottom of the fixed half of the asphalt specimen were attached to rigid plates. To provide additional support against potential lift of the fixed half of the asphalt specimen, an additional plate was placed atop this half and secured with threaded rods and nuts. This plate was positioned to rest on top of the asphalt specimen and exert no pressure on the asphalt. Also, no epoxy was used between this plate and asphalt specimen. Several trial tests were carried out confirming the suitability of the bond between the metal plates and asphalt specimens.

Load Application

An initial approach involved applying the load at the center of the plate that is attached to the top of the moving half of the asphalt specimen. However, trial tests conducted using this setup resulted in bending deflections in the asphalt specimen. Moreover, the bending of the asphalt specimen resulted in breakage of the epoxy and thus debonding of the asphalt from metal plates. The final setup addressed this difficulty by selecting the load application point right next to the shear plane. As presented in Fig. 4, the final design involved application of the load on a

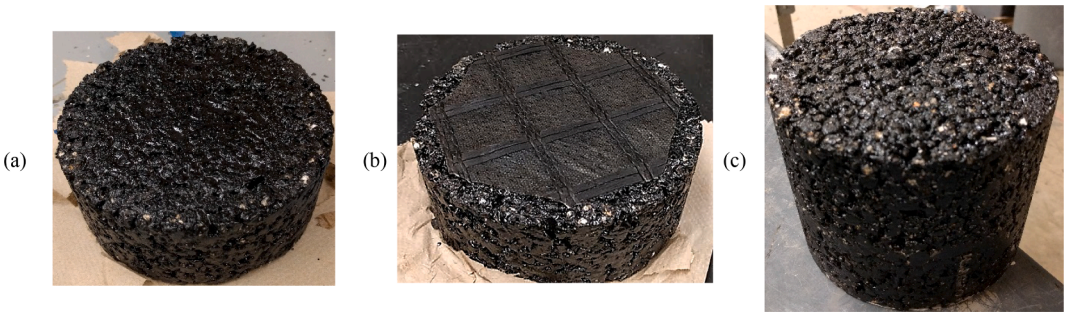

Fig. 5. Stages in asphalt sample preparation: (a) Tack coat applied on top of the bottom half; (b) paving interlayer placed over tack coat; and (c) top half placed over paving interlayer (final specimen).

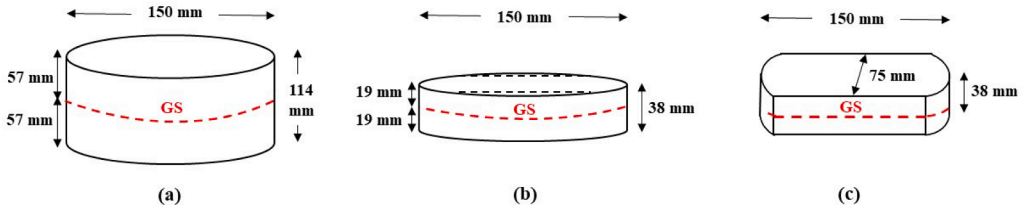

Fig. 6. Schematic of brick-shaped specimen preparation: (a) cylindrical sample (before trimming); (b) cylindrical sample (after trimming top and bottom); (c) final brick-shaped specimen.

20-mm wide base starting 10 mm from the shear plane.

Restraint on Lateral Displacement

Evaluations were conducted to determine whether the experimental design should restrict lateral displacements of the asphalt specimen during loading. Efforts in initial configurations aimed at suppressing essentially all lateral displacements so that performance would be evaluated under pure shear. It was later deemed necessary to allow lateral displacements to allow load mobilization in the geosynthetic reinforcement. Specifically, since the shear stiffness of the planar geosynthetic reinforcements used in this study was negligible, development of tension in the reinforcements was key to realize their benefits. However, mobilization of the tension in the reinforcement requires its elongation. Imposing a full restriction on lateral displacements and consequently forcing displacements to develop only in the vertical direction (i.e., perpendicular to the reinforcement plane) would minimize the contribution of reinforcements.

Allowing the asphalt specimen to displace laterally was also deemed to be more consistent with the shear mobilization in pavement surfaces under field conditions. As the shear displacement develops in the asphalt, cracks are expected to initiate along the weakest asphalt plane. The initial shear displacements along the crack plane, results a local inclination (kink) in the initially horizontal reinforcement. The asphalt surfaces on the opposite sides of the crack plane then slide over one another, resulting in dilation in the direction normal to the crack. The displacements in the direction normal to the crack lead to mobilization of the interface shear (bonding) between the reinforcement and asphalt material and, thus, the development of tension in the reinforcement. Tension development in the reinforcement has two effects on the response to the cross-shear load. The component of the reinforcement tension that is normal to the crack increases the normal stress acting on the shear plane and therefore resists propagation of the crack and its potential opening. On the other hand, the component of the reinforcement tension that is in the direction of the crack directly opposes the cross-shear load.

Final Test Procedure

Previous literature on experimental evaluation of asphalt specimens has indicated that both displacement- and load-controlled loading schemes have been successfully used in the past (e.g., [13,21,20,22,27,33,35]. In this study, after experimentally evaluating several loading schemes, a displacement-controlled approach with loading characteristics within the typical range of past research was adopted. Specifically, two loading schemes were used including a monotonic and a cyclic (relaxation) test. The monotonic test involved applying an initial seating load of 100 N, followed by loading at a constant displacement rate of 7.68 mm/min. The cyclic test included a two-stage sinusoidal load applied at a frequency of 1 Hz. Stage 1 (Small Displacements) involved loading specimens under a comparatively smaller displacement amplitude of 0.35 mm (equivalent to 0.9 % relative shear displacement), while Stage 2 (Large Displacements) involved loading with a comparatively larger displacement amplitude of 0.7 mm (equivalent to 1.8 % relative shear displacement). It should be noted that since appropriate height cannot be defined for calculation of shear strain, the relative shear displacement was used to report shear progress. The relative shear displacement was defined as the ratio between the shear displacement and the asphalt specimen thickness. A seating relaxation test involving a displacement amplitude of 0.2 mm (equivalent to 0.5 % relative shear displacement) was also applied prior to the two main testing stages. The applied load was recorded using a load cell connected to the loading rod that was attached to the moving half of the specimens. The vertical and horizontal displacements in the moving half of the specimen were monitored using two LVDTs that were connected to the loading rod and to the side of the steel plate that was connected to the moving half, respectively. Photogrammetry was also used to evaluate the development of cracks and failure modes in the asphalt specimens.

Experimental Program

Test Plan

Following establishment of the final test procedure, a monotonic and two cyclic cross-shear tests were conducted on five different interface configurations including a control (unreinforced) and four geosynthetic-reinforced specimens. Geosynthetic reinforcements included two polymeric and two glass reinforcements. All tests were conducted according to the final test procedure elaborated in the previous section and at a controlled laboratory temperature of 22 °C using an electro-hydraulic digital servo control loading machine. The machine was capable of applying displacement-controlled static and comparatively high-frequency dynamic loads. This section presents the materials that were used in the experimental program along with the obtained results.

Materials

Characteristics of materials used in the experiments are presented below.

Asphalt Mixture and Tack Coat

A dense graded asphalt mixture was used to prepare the unreinforced and geosynthetic-reinforced asphalt specimens for monotonic and cyclic cross-shear tests. The aggregates were made of angular-particle crushed stone and classified as A-1-a, in accordance with AASHTO classification (AASHTO M145 [1]; ASTM D3282 [3]). The particle size distribution curve for the aggregate is shown in Fig. 7. The maximum and nominal aggregate sizes for this aggregate were 12.5 and 9.5 mm, respectively. A Performance Grade (PG) 76–22 binder at an optimum binder content of 6.5 % was used with specific gravity of approximately 1.0. The bulk unit weight and air void content of the asphalt specimens were 21.8 kN/m^3 and 7 %, respectively.

A cationic high-float rapid-setting emulsion with a comparatively high viscosity and 3 % polymer content (CHFRS-2P) was applied as tack coat between the two lifts of asphalt layers. This tack coat had a specific gravity of 1.03, was in liquid state, and consisted of 50–70 % asphalt, 20–40 % water, and less than 1 % hydrochloric acid. The tack coat emulsion was applied at a uniform rate of 0.55 – 0.66 l/m^2 (equivalent of

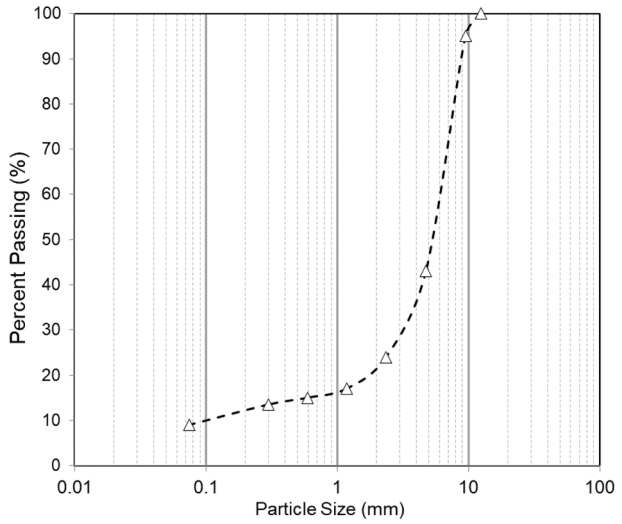

Fig. 7. Particle size distribution curve for aggregates in the mix design.

0.33 – 0.40 l/m^2 residual bitumen) in all specimens (Fig. 5a). An emulsion breaking time of about 2 hours was adopted based on prior trials.

Paving Interlayers

Four different geosynthetic reinforcements including two polymeric and two fiberglass reinforcements were used in the experimental program. The polymeric reinforcements included a polyvinyl alcohol (PVA) grid with an ultimate tensile strength of 50 kN/m (at 6 % strain) and tensile strength of 22 kN/m at 3 % strain in both machine and cross-machine directions; and a polyester (PET) grid with an ultimate tensile strength of 50 kN/m (at 12 % strain) and a tensile strength of 12 kN/m at 3 % strain in both machine and cross-machine directions. The nominal grid aperture sizes for both reinforcements were 40 × 40 mm. Both reinforcements were backed with an ultra-lightweight nonwoven fabric to facilitate field installation. The fiberglass reinforcements included a glass grid with an ultimate tensile strength of 50 kN/m (at 3 % strain), referred to as Glass 1, and a glass grid with an ultimate tensile strength of 100 kN/m (at 3 % strain), referred to as Glass 2. Both products had the same ultimate tensile strength in their machine and cross-machine directions. The nominal grid aperture sizes for both reinforcements were 30 × 30 mm and both reinforcements were backed with an ultra-lightweight nonwoven fabric to facilitate field installation.

Table 1 reports the main characteristics of all the polymeric and fiberglass reinforcements adopted in this study. Fig. 8 shows example pictures of the four reinforcement materials used in the experimental program.

Table 1
Characteristics of geosynthetic reinforcements.

Property		Test Method	PET	PVA	Glass 1	Glass 2
Mass/unit area (g/m^2)		ASTM D5261	270	210	320	596
Aperture size (mm)		Measured	40 × 40	40 × 40	30 × 30	30 × 30
Tensile Strength	MD (kN/m)	ASTM D6637	50	50	50	100
	CD (kN/m)	ASTM D6637	50	50	50	100
Tensile strength at 3 % strain (kN/m)		ASTM D6637	12	22	–	–
Elongation at failure (%)		ASTM D6637	12	6	3	3
Asphalt retention capacity (l/m^2)		ASTM D6140	0.47	0.47	0.47	0.47

Note: MD = Machine Direction; CD = Cross Machine Direction.

All reinforcements were cut to fit into the 150-mm-diameter circular cross section of the asphalt specimens (Fig. 5). Specifically, to uniformly maintain the same number of reinforcing elements (longitudinal and transverse ribs) within all reinforced specimens, reinforcements were cut to include five full apertures, as shown in Fig. 5b.

Results

Control (Unreinforced) Specimens

The results obtained in the monotonic tests conducted on an unreinforced asphalt specimen are shown in Figs. 9 and 10. The shear stress in the figure corresponds to the shear load divided by the cross-sectional area of each specimen (average shear stress) while the relative shear displacement (reported as a percentage) corresponds to the shear displacement (applied in the vertical direction) divided by the specimen thickness.

As presented in Fig. 9, the peak shear strength recorded in the monotonic test was approximately 1,400 kPa measured at a relative shear displacement of approximately 5 %. After reaching the peak strength, the asphalt specimen showed a brittle response, characterized by a rapid shear strength drop, with 150 kPa being reached at approximately 15 % relative shear displacement. Apparent cross-shear energy per sectional area was calculated as the area under the load–displacement curve divided by the specimen cross-sectional area (Fig. 10). The apparent pre-cracking energy per sectional area, obtained from the shear energy up to the peak shear strength, was approximately 1.85 kN.m/m^2. On the other hand, the apparent fracture energy per sectional area, obtained by the area under the entire recorded load–displacement curve (up to 30 % relative shear displacement), was 4.4 kN.m/m^2, less than 2.5 times the apparent pre-cracking energy.

Fig. 11 displays images captured at various testing stages. Fig. 11a corresponds to the relative shear displacement of approximately 2 % where the asphalt specimen was intact without visible cracks. The shear strength at 2 % relative shear displacement was approximately 850 kPa, corresponding to an apparent stiffness modulus (defined as the ratio between the shear strength and relative shear displacement) of 43 MPa. At the relative shear displacement of 5 %, which corresponds to the peak shear strength, the specimen was fully cracked (Fig. 11b) and the apparent stiffness modulus dropped to 28 MPa. At this point, the maximum crack opening was measured at approximately 4.5 mm. Fig. 11c shows an image of the asphalt specimen captured at 15 % relative shear displacement, when the shear strength dropped to approximately 10 % of its peak value, and the maximum crack opening increased to approximately 10.5 mm.

The results of two repeat cyclic relaxation tests on unreinforced asphalt specimens are presented in Fig. 12. As the figure shows, the results obtained in the two repeat tests were consistent with one another. The apparent dynamic cross-shear modulus in each cycle was defined as the ratio between the shear strength amplitude and relative shear displacement amplitude in that cycle. The apparent dynamic cross-shear modulus versus the number of load cycles is presented for Stage 1 (small displacement amplitudes) and Stage 2 (large displacement amplitudes) in Fig. 12a and 12b, respectively.

The apparent dynamic cross-shear moduli in the two repeat tests were approximately 510 and 660 kPa at the beginning of Stage 1, and 290 and 360 kPa at the beginning of Stage 2. The residual apparent dynamic cross-shear moduli were significantly lower at the end of each loading stage (approximately 90 kPa at the end of Stage 1 and 40 at the end of Stage 2). Inspection of the data trends presented in Fig. 12 indicates a comparatively lower rate of modulus degradation for small displacement amplitudes (Fig. 12a) as compared to large displacement amplitudes (Fig. 12b).

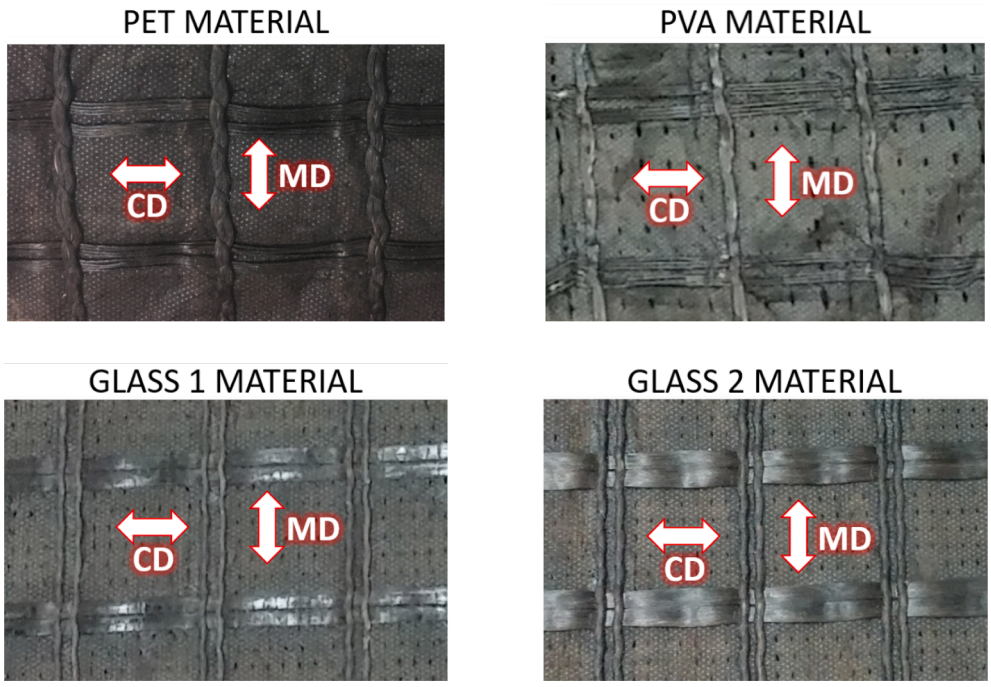

Fig. 8. Photographs of the four geosynthetic materials.

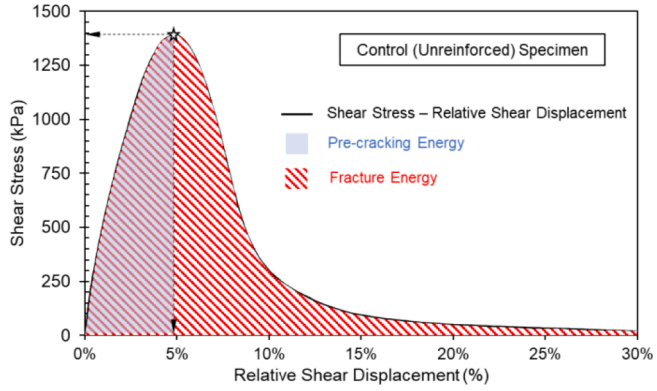

Fig. 9. Shear stress versus relative shear displacement for unreinforced asphalt in monotonic cross-shear test.

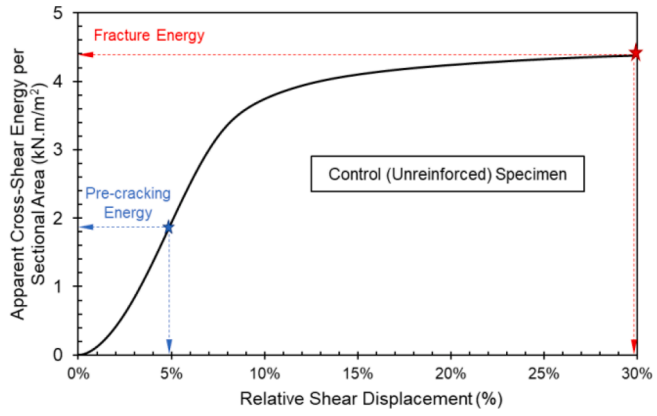

Fig. 10. Apparent shear energy in unreinforced asphalt.

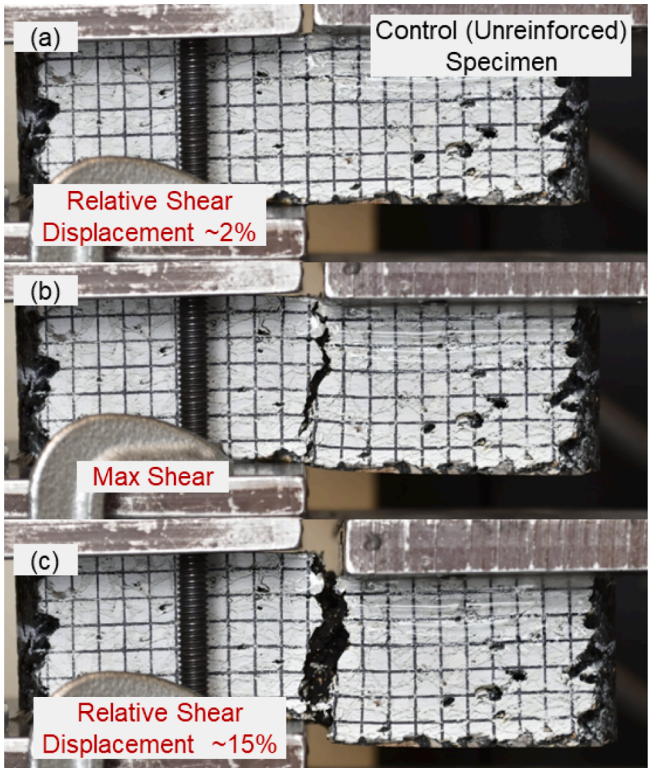

Fig. 11. Images of the unreinforced asphalt during monotonic cross-shear test: a) at 2% relative shear displacement; b) at max shear stress; and c) at 15% relative shear displacement.

Polymer-reinforced Specimens

Fig. 13 summarizes the results of the monotonic cross-shear tests on polymer-reinforced asphalt specimens as compared to the control (unreinforced) specimen. The peak shear strength recorded for both

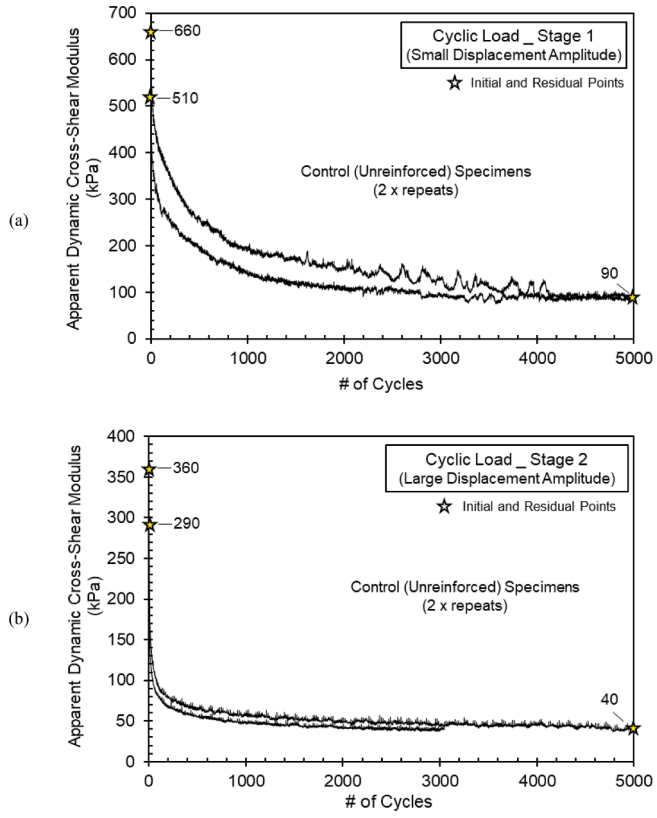

Fig. 12. Results of cyclic cross-shear test in unreinforced asphalt: a) Stage 1 (small displacement amplitude); b) Stage 2 (large displacement amplitude).

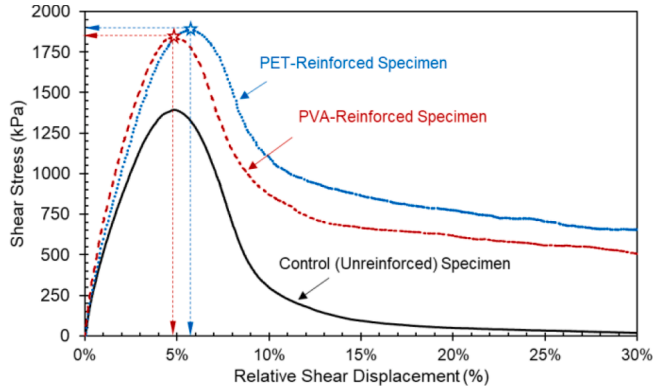

Fig. 13. Shear stress versus relative shear displacement for polymer-reinforced asphalt in monotonic cross-shear test.

polymer-reinforced specimens was very similar (1,850 and 1,900 kPa in PVA- and PET-reinforced specimens, respectively) but significantly higher than that recorded for the unreinforced specimen. However, the relative shear displacement corresponding to the peak shear strength in both polymer-reinforced specimens was similar to that in the unreinforced specimen (approximately 5 % in the PVA-reinforced and 6 % in the PET-reinforced specimens). The apparent pre-cracking energy for the PVA- and PET-reinforced specimens was determined as 2.1 and 2.4 kN.m/m^2, respectively, which is approximately 15 % to 30 % higher than that determined for the unreinforced specimen (Fig. 14).

In contrast to the unreinforced specimen, both polymer-reinforced specimens showed a significant residual shear strength after the peak, indicating a comparatively flexible post-cracking behavior and comparatively high apparent fracture energy. At 15 % relative shear displacement, the shear strength values in the PVA- and PET-reinforced

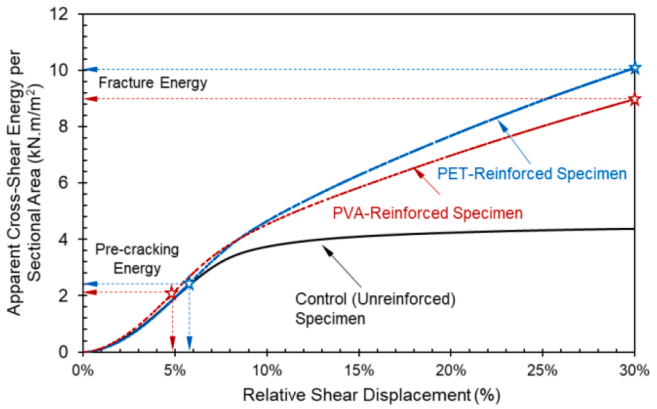

Fig. 14. Apparent cross-shear energy in polymer-reinforced asphalt.

specimens were approximately 650 kPa and 850 kPa, respectively. In addition, the apparent fracture energy per sectional area corresponding to 30 % relative shear displacement was approximately 9 and 10 kN.m/m^2 in the PVA- and PET-reinforced specimens, respectively. This is more than twice the apparent fracture energy in the unreinforced specimen and over four times the apparent pre-cracking energy in the polymer-reinforced specimens (Fig. 14).

Images of the polymer-reinforced specimens during various stages of the monotonic cross-shear test are presented in Fig. 15. At the relative shear displacements around 2 % (Fig. 15a) both reinforced specimens were seemingly intact without visible cracks, similar to the unreinforced specimen. However, the images corresponding to peak shear strengths exhibited significantly less severe cracking in the polymer-reinforced specimens (Fig. 15b) as compared to that in the unreinforced specimen (Fig. 11b). The apparent stiffness modulus at 2 % was calculated as 50 and 56 MPa in the PVA- and PET-reinforced specimens, respectively. At 15 % relative shear displacement, fully developed cracks were observed in both polymer-reinforced specimens (Fig. 15c). However, the maximum crack openings in the reinforced specimens were measured at approximately 5 and 3.5 mm for the PVA- and PET-reinforced specimens, respectively, which were significantly smaller than that measured in the unreinforced specimen.

Similar to the unreinforced asphalt, two repeat cyclic relaxation tests were conducted using polymer-reinforced asphalt specimens, the results of which are presented in Fig. 16. The apparent dynamic cross-shear modulus values obtained in all four tests conducted on polymer-reinforced specimens were consistently higher than those obtained on the unreinforced specimens in both testing stages. With the exception of one repeat test on PET-reinforced specimens under small displacement amplitudes, consistent results were observed in tests on polymer-reinforced specimens. The average apparent shear moduli at the beginning of Stage 1 were 705 and 780 kPa in the PVA- and PET-reinforced specimens, respectively. At the beginning of Stage 2, the values were 520 and 480 in the PVA- and PET-reinforced specimens, respectively. These results also reveal a significantly higher initial apparent dynamic cross-shear modulus in the polymer-reinforced specimens as compared to that in the unreinforced specimens (values approximately 20 % to 35 % higher in Stage 1 and 50 % to 60 % higher in Stage 2). The residual apparent dynamic cross-shear modulus, measured at the end of each stage, showed even higher values in the polymer-reinforced specimens as compared to those in the unreinforced specimens. The average apparent shear moduli in the PVA- and PET-reinforced specimens at the end of Stage 1 were 240 and 250 kPa, respectively, and at the end of Stage 2 were 125 and 110 kPa, respectively. Such results indicate that the residual apparent dynamic cross-shear moduli in the polymer-reinforced specimens were at least 2.7 times greater than in the unreinforced specimens.

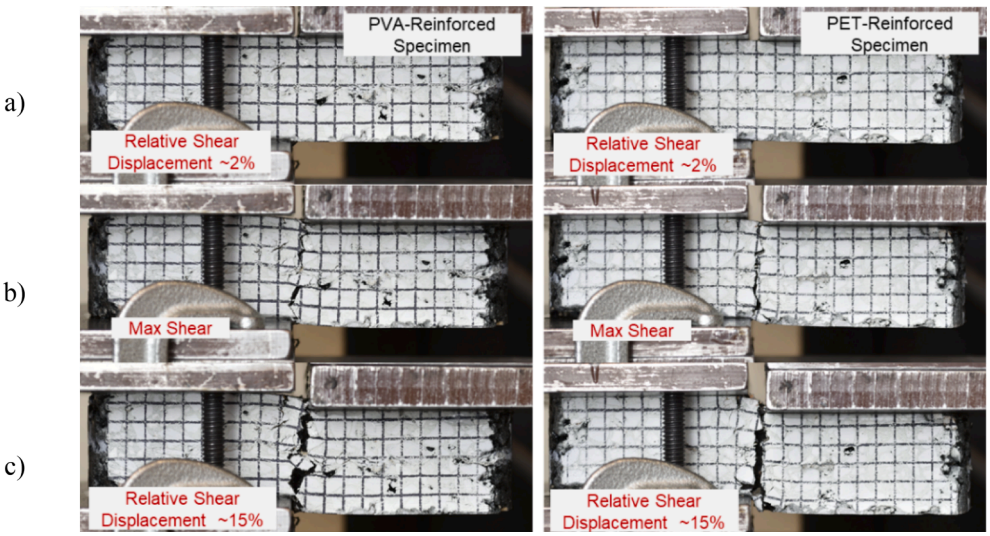

Fig. 15. Images of polymer-reinforced asphalt specimens in monotonic cross-shear tests: a) at 2% relative shear displacement; b) at max shear stress; and c) at 15% relative shear displacement.

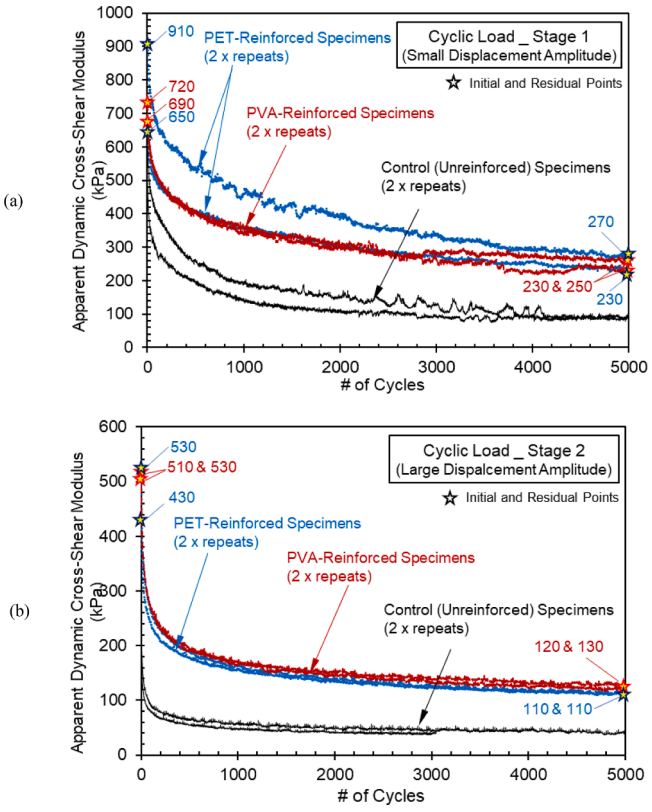

Fig. 16. Results of cyclic cross-shear tests in polymer-reinforced asphalt: a) Stage 1 (small displacement amplitude); and b) Stage 2 (large displacement amplitude).

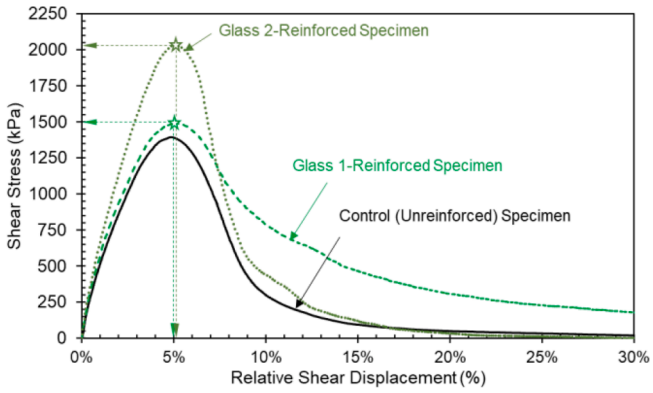

Fig. 17. Shear stress versus relative shear displacement for glass-reinforced asphalt in monotonic cross-shear test.

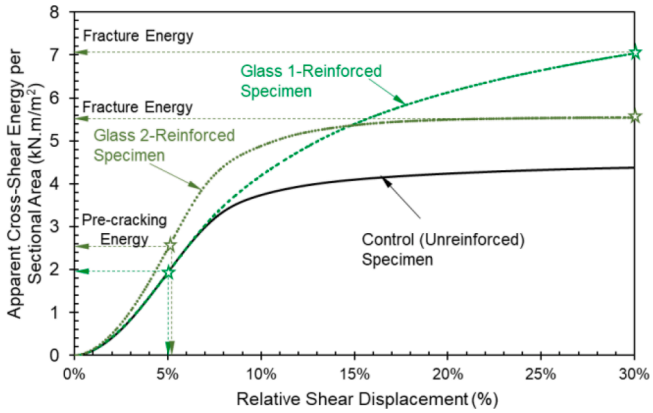

Fig. 18. Apparent cross-shear energy in glass-reinforced asphalt.

Glass-reinforced Specimens

The results of the monotonic cross-shear tests conducted on glass-reinforced specimens are presented in Figs. 17 and 18. As shown in these figures, both glass-reinforced specimens exhibited an enhanced response as compared to the unreinforced specimen. However, the benefits observed among the two glass reinforcements differed. The specimen reinforced with Glass 2, which was significantly stiffer and had twice the ultimate tensile strength of Glass 1, showed a significantly higher peak shear strength than the unreinforced specimen and, consequently, significantly greater apparent pre-cracking energy. Similar to the unreinforced specimen, the specimen reinforced with Glass 2 showed a significant post-peak shear strength drop, thus, negligible residual shear strength and hence little increase in post-cracking (fracture) energy. The specimen reinforced with Glass 1, the

less stiff glass, showed a modest increase in peak shear strength, but a more significant residual shear strength. Consequently, the specimen reinforced with Glass 1 exhibited similar apparent pre-cracking energy as the unreinforced specimen, but higher apparent fracture energy than the unreinforced specimen.

Failure patterns, as observed from images captured during the monotonic cross-shear tests on glass-reinforced specimens, were similar to those observed in the polymer-reinforced specimens. The specimens remained intact at comparatively small relative shear displacements (Fig. 19a). At peak shear strength, although cracks were visible in the two glass-reinforced specimens (Fig. 19b), the severity of those cracks was significantly less than that in the cracks observed at peak shear strength in the unreinforced specimen (Fig. 11b). At 15 % relative shear displacement, both specimens were severely cracked, with a maximum crack opening exceeding 5 mm (Fig. 19c).

The apparent dynamic cross-shear moduli obtained in the two repeats of cyclic relaxation cross-shear tests on glass-reinforced specimens are presented in Fig. 20. The response under loading Stage 1, in which relative shear displacements were comparatively small, was found to be similar for both glass-reinforced specimens (Fig. 20a). In this stage, the average initial apparent moduli in the glass-reinforced specimens were approximately 665 and 630 kPa for specimens reinforced with Glass 1 and Glass 2, respectively, corresponding to values approximately 10 % to 15 % higher than those in the unreinforced specimens. The residual apparent moduli, measured at the end of Stage 1, were approximately 185 and 165 kPa for specimens reinforced with Glass 1 and Glass 2, respectively, corresponding to approximately twice the value obtained in the unreinforced specimens.

In loading Stage 2, in which comparatively higher relative shear displacements were used, the specimens reinforced with Glass 1 (less stiff) exhibited a comparatively better response than the specimens reinforced with Glass 2 (stiffer) (Fig. 20b). Nonetheless, the specimens reinforced with Glass 2 still exhibited a considerably better performance than the unreinforced specimens. The average initial and residual apparent dynamic cross-shear moduli in this loading stage were approximately 505 and 100 kPa in Glass 1-reinforced specimens, respectively, and approximately 475 and 80 kPa in Glass 2-reinforced specimens, respectively.

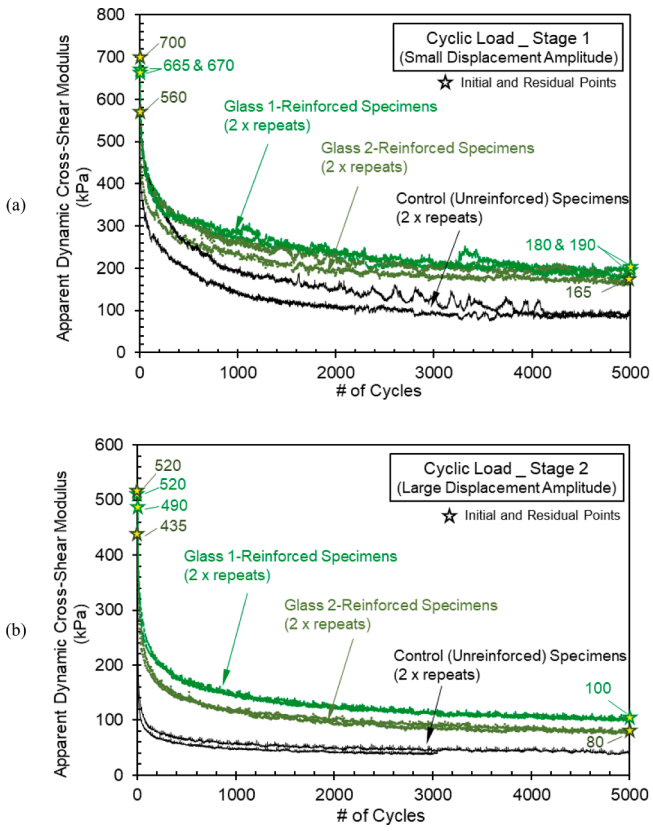

Fig. 20. Results of cyclic cross-shear tests in glass-reinforced asphalt: a) Stage 1 (small displacement amplitude); and b) Stage 2 (large displacement amplitude).

Discussions

Mechanisms of Cross-Shear Resistance

An evaluation of the results collected during monotonic cross-shear tests suggests that although the reinforcement interlayers enhanced the pre-cracking response of asphalt under cross-shear loading, the most significant benefit from reinforcements relates to their enhanced post-

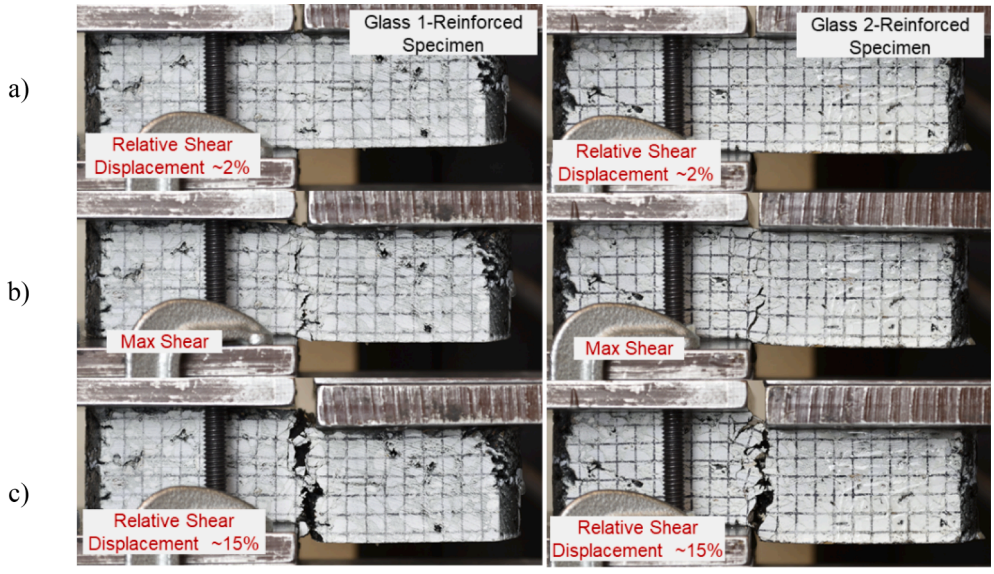

Fig. 19. Images of glass-reinforced asphalt specimens in monotonic cross-shear test: a) at 2% relative shear displacement; b) at max shear stress; and c) at 15% relative shear displacement.

cracking response, particularly for polymeric reinforcements. Specifically, incorporation of a reinforcement interlayer provides a flexible post-crack behavior characterized by a comparatively high residual shear strength and high fracture energy as compared to unreinforced asphalt. These results indicate that the presence of reinforcement interlayers in asphalt helps not only to retard the initiation of cross-shear cracks, but, more importantly, to mitigate propagation of such cracks.

The testing program allowed identification of the key characteristics of reinforcements that govern the enhanced performance over unreinforced asphalt. Specifically, evaluation of the results from the monotonic cross-shear tests underlines the significance of the reinforcement tensile stiffness in the benefits realized from asphalt reinforcement under cross-shear loading. The polymeric and glass reinforcements used in this study span a wide range of tensile stiffness values. Fig. 21 schematically displays simplified unit tension-strain data, reported by the manufacturers, for the four geosynthetics used in this study. This data can be used to compare the tensile stiffness of the various reinforcement products. The PET reinforcement had the lowest tensile stiffness of the four reinforcements, while the PVA reinforcement had approximately twice the tensile stiffness of the PET. The tensile stiffness of Glass 1 was twice that of the PVA. The highest stiffness among the four materials was that of Glass 2, which was approximately twice as stiff as Glass 1. An evaluation of the data presented in the previous sections indicates that, in terms of fracture energy, the polymer-reinforced specimens (PET- and PVA-reinforced specimens) exhibited comparatively better performance than the specimens reinforced with either glass grid. Accordingly, the comparatively lower stiffness of the polymeric reinforcement may have resulted in higher compatibility with the asphalt properties in its post-cracking stage, helping mitigate propagation of cracks. The specimen reinforced with the stiffest reinforcement (Glass 2) showed the highest peak shear strength across all specimens, resulting in a delayed initiation of cracking. However, the same specimen showed essentially no residual cross-shear resistance, indicating no benefits in mitigating propagation of cracks.

An evaluation of the lateral displacement data obtained in the monotonic cross-shear tests on PET- and glass-reinforced specimens as well as unreinforced specimens reveals additional information on the mechanisms that govern the response during cross-shear testing. The lateral displacements of the moving half of all specimens, except for the PVA specimen, were measured using an LVDT that was connected to the rigid plate attached to this half. The relative lateral displacements were calculated by dividing the lateral displacements by the length of the reinforcement, and quantifies the relative movement of the loaded half-specimen in relation to the stationary half-specimen as cross-shearing progresses. Fig. 22 shows the relative lateral displacement versus relative shear displacement curves, as obtained for the various monotonic tests. The relative lateral displacements were expected to significantly impact the tension development in the reinforcement interlayers: the larger the relative lateral displacement, the higher the developed

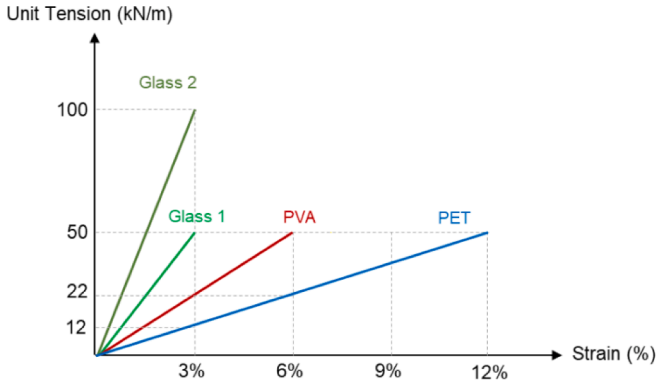

Fig. 21. Tensile characteristics of polymeric and glass reinforcements.

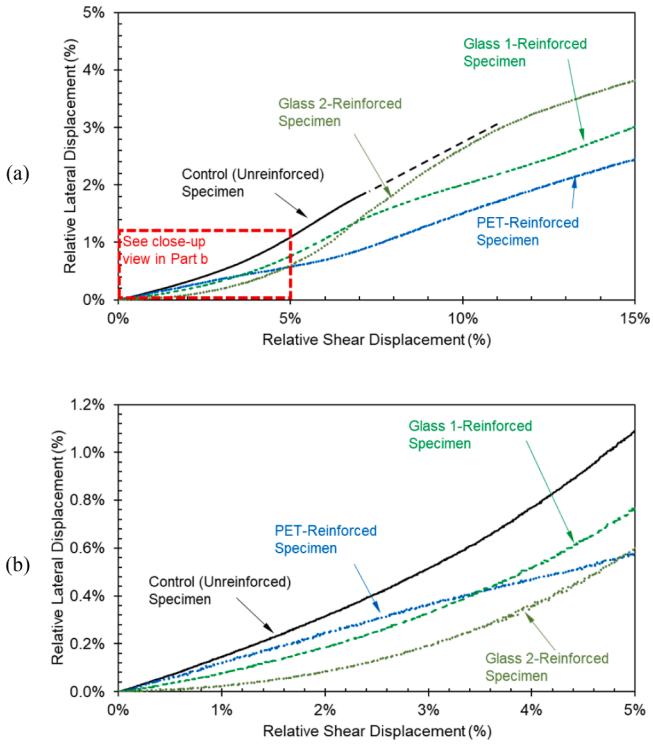

Fig. 22. Relative lateral displacements in cross-shear tests: a) entire test; and b) close-up of pre-cracking phase.

tension in the reinforcement. However, the reinforcement tension should eventually transfer to the surrounding asphalt through shear. Therefore, during cross-shear loading, two phases of asphalt-reinforcement interaction can be identified, as follows:

1) Before full formation of cross-shear cracks (pre-cracking phase), while relative shear displacements are comparatively small, the tensile stiffness of the reinforcement governs the overall performance of the asphalt-reinforced specimen; accordingly, a comparatively stiff reinforcement develops higher tension than a reinforcement with comparatively lower stiffness. Thus, under small relative shear displacements (e.g., less than 5 %), the specimen reinforced with Glass 2 (i.e., the stiffest reinforcement in this study) developed the highest reinforcement tension, resulting in the highest shear stress (Fig. 17) and, consequently, the lowest relative lateral displacements (Fig. 22b). During this phase, the comparatively high tension developed by the stiffer reinforcement maintained the specimen integrity and controlled its lateral displacements. On the other hand, the specimen reinforced with PET (the least stiff reinforcement in this study) showed the highest relative lateral displacements, with a trend mostly similar to that of the unreinforced specimen (Fig. 22b).
2) After full development of cross-shear cracks (i.e., during the post-cracking phase), where comparatively large relative shear displacements had occurred, the asphalt on the two sides of the crack planes are almost separated while geosynthetic reinforcement still holds the two half-specimens connected. Accordingly, the additional shear displacements will be carried only by the reinforcement interlayer, forcing it to break or fail in pullout mode. Therefore, instead of the reinforcement tensile stiffness, the performance will be governed by the reinforcement elongation at break (in case the reinforcement breaks) or bonding strength between asphalt and reinforcement (in case the reinforcement fails in pullout mode). The data presented in Fig. 22a is consistent with this interpretation, as it shows a marked change in the response of the reinforced asphalt specimens after

approximately 5 % relative shear displacement, when cross-shear cracks have fully developed. Specifically, the Glass 2-reinforced specimen, which showed the lowest relative lateral displacement before cracking, developed lateral displacements at a faster rate than the other specimens. Moreover, the trend of additional lateral displacements developed in the Glass 2-reinforced specimen became similar to that in the unreinforced specimen, indicating a declining contribution of Glass 2 to the overall performance under comparatively large relative shear displacements. In fact, beyond the relative shear displacement of 10 %, the relative lateral displacement curves of the Glass 2-reinforced specimen and unreinforced specimen merge. This merging point corresponds to approximately 3 % relative lateral displacement, which is close to the elongation at break of the Glass 2 material. In contrast, the PET- and Glass 1-reinforced specimens continued to maintain residual resistance even beyond the relative shear displacement of 10 % (Figs. 13 and 17), which is consistent with the comparatively less relative lateral displacements for PET- and Glass 1-reinforced specimens in Fig. 22a.

Degradation of Dynamic Shear Modulus

To better understand the benefits derived from reinforcement interlayers in mitigating the degradation of dynamic cross-shear modulus, the data obtained in the cyclic tests were reevaluated using normalized results in which the modulus obtained in each cycle was divided by the maximum modulus obtained in the first cycle. The resulting normalized data for all tests are shown for loading Stages 1 and 2 in Fig. 23a and 23b, respectively. Although all reinforcements evaluated in this study showed a reduced degradation rate of the apparent dynamic cross-shear modulus, differences among the responses of various reinforcements could be observed and are discussed here.

The responses of reinforced asphalt specimens under cyclic loads are affected not only by the tensile properties and bond strength of reinforcements but also, and more importantly, by characteristics of the reinforcement materials under fatigue conditions. Specifically, since the shear displacement amplitudes used in the cyclic tests were comparatively small as compared to that resulted the peak shear strength in monotonic tests, the reinforcement responses under fatigue conditions are expected to govern the overall performance of the reinforced specimens in cyclic tests. Although the reinforcement materials selected for this study were not independently evaluated under fatigue conditions, previous studies on the response under fatigue of the same or similar materials have been revealing. Specifically, Montestruque et al. [20] evaluated the response of the same PET and glass materials selected for this study using fatigue test equipment developed at the University of Sao Paulo. The results of these fatigue tests, which were conducted under differential vertical movement (shear mode) similar to that adopted in this study, indicated a comparatively better fatigue performance of the PET yarns as compared to the glass yarns. Observations from the cyclic tests conducted in this study are consistent with the findings reported by Montestruque et al. [20]. As presented in Fig. 23, in both small- and large-amplitude loading stages, the polymeric reinforcements exhibited better performance than the glass reinforcements in terms of retarding the degradation rate of apparent dynamic cross-shear modulus in the asphalt specimens. In Stage 1, the apparent dynamic cross-shear modulus degraded by approximately 85 % in the unreinforced asphalt, whereas the degradation of this modulus in the glass-reinforced asphalt ranged from 70 to 75 %, while in the polymer-reinforced asphalt it ranged from 65 to 70 %. In Stage 2, the same number of cycles resulted in a modulus degradation of approximately 90 %, 80 to 85 %, and 75 to 80 %, in the unreinforced, glass-reinforced and polymer-reinforced specimens, respectively.

The same data displayed in Fig. 23 are plotted in logarithmic scale in Fig. 24 to better evaluate the modulus degradation trends of the various

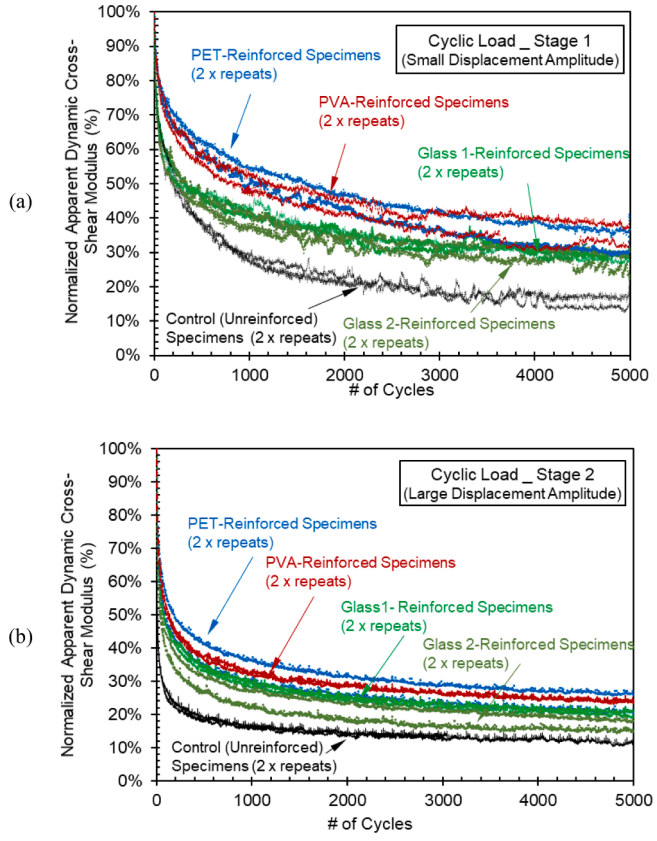

Fig. 23. Degradation of modulus in cyclic cross-shear tests: a) Stage 1 (small displacement amplitude); and b) Stage 2 (large displacement amplitude).

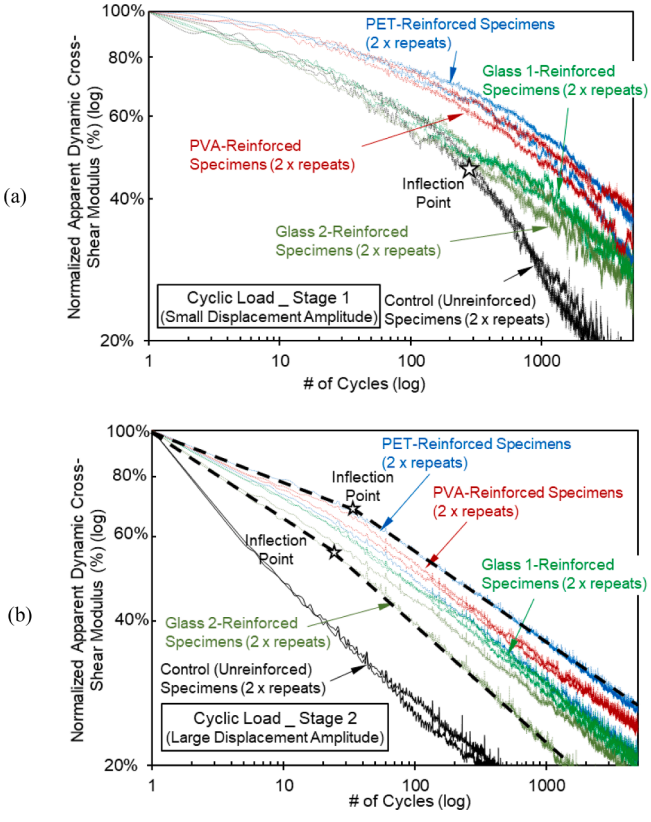

Fig. 24. Degradation of modulus in cyclic cross-shear tests in logarithmic scale: a) Stage 1 (small displacement amplitude); and b) Stage 2 (large displacement amplitude).

specimens. The nonlinear trend of apparent modulus degradation in Stage 1 (Fig. 24a) is similar to typical modulus degradation trends reported using other test procedures (e.g., four point bending beam tests) on reinforced and/or unreinforced asphalt (e.g., [22]. However, with the exception of the unreinforced specimen, an inflection point was not observed in any of the specimens. The inflection point in the unreinforced asphalt was observed at approximately 300 load cycles, indicating that cracking begins to significantly propagate after this cycle. The modulus degradation curves of glass-reinforced asphalt specimens were similar to those of the unreinforced specimens up to the inflection point, indicating the contribution from glass reinforcements was likely small prior to this point. However, following the inflection point, the unreinforced specimens degraded at a significantly faster rate than the glass-reinforced specimens.

The modulus degradation in the unreinforced specimens under large-amplitude cyclic loading (Stage 2) was comparatively more significant and revealed a different trend as compared to Stage 1. As presented in Fig. 24b, the degradation of the unreinforced specimens in loading Stage 2 followed a reasonably linear trend at a significantly higher rate than the reinforced specimens. The reinforced specimens showed bilinear degradation trends with potential inflection points ranging from 25 to 40 cycles. The modulus degradation rate was comparatively higher in the glass-reinforced specimens than the polymer-reinforced specimens.

Implications

Consistent with previously stated objectives, this study aimed at: (1) conceiving a loading scheme (i.e., cross-shear loading) that evaluates an important mechanism mobilized by geosynthetic reinforcements within asphalt, (2) developing a new experimental setup for the conceived loading scheme, (3) developing relevant parameters and protocols to evaluate experimental data, and (4) demonstrating that the proposed experimental procedure is practical and capable of identifying differences among various interface configurations. Findings of this study is expected to facilitate continued research on important, yet comparatively less studied, cross-shear testing of unreinforced and geosynthetic-reinforced asphalt layers. While the study did not aim at establishing a standard test procedure at this point, the proposed test procedure may prove helpful for additional evaluations. Full implementation of the test procedure developed herein into a standard requires complementary testing programs with multiple repeats of the various interface configurations. In addition, establishing statistical difference between the performances of various interface configurations requires applying statistical techniques such as T-tests, ANOVA, and/or Tukey's range test. However, such extensive testing program to standardize the proposed test is beyond the scope of this paper.

Conclusions

A new test procedure was developed to evaluate the benefits derived from reinforcement interlayers incorporated within the asphalt layers under cross-shear loading. This test produces experimental data under shear stresses that are applied perpendicular to the geosynthetic reinforcement plane, an important source for reflective cracking with only limited previous research. The developed test involved both monotonic and cyclic loading modes that led to specific parameters defined to evaluate the test results. Average cross-shear stress and apparent cross-shear energy per sectional area were used to interpret the monotonic test data, and apparent dynamic cross-shear modulus was defined to interpret cyclic test results. Preliminrary cross-shear test results on unreinforced asphalt specimens as well as asphalt specimens that were reinforced using two polymeric and two glass reinforcement materials showed capability of the experimental procedure to underline geosynthetic benefits as reinfrocement interlayers. All reinforcements tested in this study were found to enhance the performance of the asphalt specimens subjected to the cross-shear load.

The monotonic cross-shear resistance in the reinforced asphalt specimens was found to be affected by several factors, including the reinforcement tensile strength and elongation at break. The contribution of the reinforcements to the performance of asphalt specimens under cross-shear loads could be evaluated in two phases: the pre-cracking phase (peak shear strength) and the post-cracking phase (residual shear strength). The response in the pre-cracking phase was found to be primarily governed by the tensile stiffness of the reinforcement material, whereas the response in the post-cracking phase was found to be governed by the elongation at breakage of the reinforcement layer. None of the reinforcements tested were found to significantly affect the relative shear displacement at the asphalt peak shear point. However, all reinforcements were observed to increase the peak cross-shear strength and apparent pre-cracking shear energy, demonstrating the capability of reinforcements to delay the initiation of cracks. The reinforcements also restrained relative lateral (i.e., normal to the crack plane) displacements and thus delayed the opening of shear cracks.

In the cyclic cross-shear tests, all reinforcements tested in this study were found to enhance the performance of the asphalt specimens subjected to small- and large-amplitude cyclic cross-shear loads. Specifically, the benefits derived from the reinforcements were observed as enhancing the initial and residual apparent dynamic modulus values as well as retarding the modulus degradation rate in the asphalt. Modulus degradation in large-amplitude cyclic tests was found to follow a linear trend in the unreinforced specimens and a bilinear trend in the reinforced specimens. The inflection point in the control (unreinforced) specimens was found to occur under small-amplitude cyclic loading at approximately 300 load cycles. In contrast, the inflection point in the reinforced specimens was found to occur under large-amplitude cyclic loading at approximately 25 to 40 load cycles.

Overall, the developed cross-shear test in this study was found practical and capable of identifying performance difference among various interface configurations. Test setup components and sample preparation are similar to those of conventional asphalt tests and can be readily adopted by research laboratories. However, full implementation of this test into a standard requires additional and extensive testing programs (including multiple repeat tests) along with statistical analyses that can statistically differentiate the performance among various interface configurations.

Declaration of Competing Interest

The authors declare that they have no known competing financial interests or personal relationships that could have appeared to influence the work reported in this paper.

Acknowledgements

The authors acknowledge the invaluable support received from Huesker, Inc. throughout the study. The help provided by Dr. Hamza Jaffal, Federico Castro, Dr. Ramez Hajj, and Chian Hen Tam in various experimental components is also greatly appreciated.

References

[1] AASHTO. (2012). "Standard specification for classification of soils and soil-aggregate mixtures for highway construction purposes." AASHTO M145-91 (12), Washington, DC.
[2] Al-Qadi, I. L., Morian, D. A., Stoffels, S. M., Elseifi, M., Chehab, G., and Stark, T. (2008). "Synthesis on use of geosynthetics in pavements and development of a roadmap to geosynthetically-modified pavements." *Federal Highway Administration*, Report DTFH61-06-P-00182.
[3] ASTM. (2015). "Standard practice for classification of soils and soil-aggregate mixtures for highway construction purposes." ASTM D3282-15, West Conshohocken, PA.
[4] Austin RA, Gilchrist AJT. Enhanced performance of asphalt pavements using geocomposites. Geotext Geomembr 1996;14:175–86.

[5] Canestrari F, Ferrotti G, Partl MN, Santagata E. Advanced testing and characterization of interlayer shear resistance. Transportation Research Record: Journal of Transportation Research Board 2005;1929:69–78.

[6] Carvalho, R. L., and Schwartz, C. W. (2013). "The importance of simulating moving wheel loads in the mechanistic analysis of permanent deformations in flexible pavements." *Proceedings of Airfield and Highway Pavement: Sustainable and Efficient Pavements,* 1156-1166.

[7] Correia NS, Zornberg JG. Mechanical response of flexible pavements enhanced with geogrid-reinforced asphalt overlays. Geosynthetics International 2016;23(3):183–93.

[8] Correia NS, Zornberg JG. Strain distribution along geogrid-reinforced asphalt overlays under traffic loading. Geotext Geomembr 2018;46:111–20.

[9] Ferrotti G, Canestrari F, Pasquini E, Virgili A. Experimental evaluation of the influence of surface coating on fiberglass geogrid performance in asphalt pavements. Geotext Geomembr 2012;34:11–8.

[10] Graziani A, Pasquini E, Ferrotti G, Virgili A, Canestrari F. Structural response of grid-reinforced bituminous pavements. Mater Struct 2014;47(8):1391–408.

[11] Ingrassia LP, Virgili A, Canestrari F. Effect of geocomposite reinforcement on the performance of thin asphalt pavements: Accelerated pavement testing and laboratory analysis. Case Stud Constr Mater 2020;12:e00342.

[12] Irwin, G. R. (1958). Fracture. *Handbuch der Physik*, Vol. 6, Springer, Berlin, 551-590. https://doi.org/10.1007/978-3-642-45887-3_5, 551-590.

[13] Khodaii A, Fallah S, Nejad FM. Effects of geosynthetics on reduction of reflection cracking in asphalt overlay. Geotext Geomembr 2009;27:131–40.

[14] Kumar, V. V., and Saride, S. (2017). "Evaluation of flexural fatigue behavior of two-layered asphalt beams with geosynthetic interlayers using digital image correlation." In *Proceedings of the Transportation Research Board 96th Annual Meeting, Washington DC, USA,* 8-12.

[15] Kumar VV, Saride S, Zornberg JG. Mechanical response of full-scale geosynthetic-reinforced asphalt overlays subjected to repeated loads. Transp Geotech 2021;30:100617. https://doi.org/10.1016/j.trgeo.2021.100617.

[16] Kumar VV, Saride S, Zornberg JG. Fatigue Performance of Geosynthetic-reinforced Asphalt Layers. Geosynthetics International 2021;28(6):584–97. https://doi.org/10.1680/jgein.21.00013.

[17] Lekarp F, Isacsson U, Dawson A. State of the Art. I: Resilient response of unbound aggregates. *J Transp Eng*, ASCE 2000;126(1):66–75.

[18] Leutner R. Untersuchung des Schichtenverbundes beim bituminosen Oberbau. Bitumen 1979;Heft 3/1979.

[19] Lytton RL. Use of geotextiles for reinforcement and strain relief in asphalt concrete. Geotext Geomembr 1989;8(3):217–37.

[20] Montestruque, G., Bernucci, L., Fritzen, M., and da Motta, L. G. (2012). "Stress relief asphalt layer and reinforcing polyester grid as anti-reflective cracking composite interlayer system in pavement rehabilitation." *Proceedings of 7th RILEM International Conference on Cracking in Pavements*, Springer, Dordrecht, 1189-1197.

[21] Montestruque, G., Rodrigues, R., Nods, M., and Elsing, A. (2004). "Stop of reflective crack propagation with the use of PET geogrid as asphalt overlay reinforcement." *In 5th Int RILEM Conf on Cracking in Pavements-Mitigation, Risk Assessment and Prevention*. Ed. by Petit, C., Al-Qadi, I., and Millien, A., 231-238.

[22] Pasquini E, Bocci M, Canestrari F. Laboratory characterization of optimized geocomposites for asphalt pavement reinforcement. Geosynthetic International 2014;21(1):24–36.

[23] Roodi, G. H., Morsy, A. M., and Zornberg, J. G. (2017). "Experimental evaluation of the interaction between geosynthetic reinforcements and hot mix asphalt." *International Conference on Highway Pavement & Airfield Technology*, ASCE, Philadelphia, PA, 428-439.

[24] Sanders PJ. Reinforced Asphalt Overlays for Pavements. University of Nottingham, UK; 2001. PhD Thesis,.

[25] Saride S, Kumar VV. Influence of geosynthetic-interlayers on the performance of asphalt overlays on pre-cracked pavements. Geotext Geomembr 2017;45(3):184–96.

[26] Saride S, Kumar VV. Estimation of service life of geosynthetic-reinforced asphalt overlays from beam and large-scale fatigue tests. J Test Eval 2019;47(4):2693–716.

[27] Sobhan K, Tandon V. Mitigating reflection cracking in asphalt overlays using geosynthetic reinforcements. Road Materials and Pavement Design 2008;9(3):367–87.

[28] Solatiyan E, Bueche N, Carter A. A review on mechanical behavior and design considerations for reinforced-rehabilitated bituminous pavements. Constr Build Mater 2020;257:119483. https://doi.org/10.1016/j.conbuildmat.2020.119483.

[29] Spadoni S, Ingrassia LP, Paoloni G, Virgili A, Canestrari F. Influence of geocomposite properties on the crack propagation and interlayer bonding of asphalt pavements. Materials 2021;14:5310. https://doi.org/10.3390/ma14185310.

[30] Virgili A, Canestrari F, Grilli A, Santagata FA. Repeated load test on bituminous systems reinforced by geosynthetics. Geotext Geomembr 2009;27:187–95.

[31] Wargo A, Safavizadeh SA, Kim YR. Comparing the performance of fiberglass grid with composite interlayer systems in asphalt concrete. Transportation Research Record: Journal of Transportation Research Board 2017;2631:123–32.

[32] West, R. C., Zhang, J., and Moore, J. (2005). "Evaluation of bond strength between pavement layers." NCAT Report 05-08, National Center for Asphalt Technology, Auburn, AL.

[33] Yin Y. Fatigue experiments of simulating propagating process of reflective cracking in asphalt concrete overlays. Applied Mechanics and Materials 2012;193–194:1454–60.

[34] Zamora-Barraza D, Calzada-Peres MA, Castro-Fresno D, Vega-Zamanillo A. Evaluation of anti-reflective cracking systems using geosynthetics in the interlayer zone. Geotext Geomembr 2011;29(2):130–6.

[35] Zhou, F., and Scullion, T. (2003). *Upgraded overlay tester and its application to characterize reflection cracking resistance of asphalt mixtures*. Report No. FHWA/TX-04/0-4467-1, Texas Transportation Institute, College Station, TX.

[36] Zofka A, Maliszewski M. Practical overlay design for geogrid reinforcement of asphalt layers. Road Materials and Pavement Design 2019;20(sup1):S163–82.

[37] Zornberg, J. G. (2017a). "Functions and applications of geosynthetics in roadways: Part 1." *Geosynthetics*, *Industrial Fabrics Association International*, February, 34-40.

[38] Zornberg, J. G. (2017b). "Functions and applications of geosynthetics in roadways: Part 2." *Geosynthetics*, *Industrial Fabrics Association International*, April, 34-40.